Design of a Robotic Rat Hindlimb Knee and Hip Focus

Grace Millick[a], Hayden Penczak[a], Wolfgang Reynolds[a], Jack Pessaud[a], Hudson Burke[b], and Shawn Russell[a,b,c]

[a] Department of Biomedical Engineering, University of Virginia
[b] Department of Mechanical Engineering, University of Virginia
[c] Department of Orthopedics, University of Virginia

Abstract

Herein, techniques to mimic the knee joint's polycentric motion and the hip's three degrees of rotational freedom are demonstrated along with rudimentary actuation techniques to create a physical model of a Lewis rat hindlimb. Three knee joints were designed: an Average ICR 4-Bar Linkage, a Three Position 4-Bar Linkage, and a Rolling Contact Joint. The knee actuation was controlled by two servos with attached cables representing knee flexor and extensor muscle groups. The hip was designed with orthogonally connected servos allowing three axis rotation and actuation. The moving instantaneous center of rotation (ICR) of three knee joint designs were compared to the ICR of a computational model and the root mean squared error (RMSE) was measured through the knee range of motion from 20 to 150 degrees between the tibia and femur. The Average ICR 4-Bar Linkage model had an average RMSE of 11.344 mm with a standard deviation of 1.048mm. The Three Position 4-Bar Linkage model had an average RMSE of 18.294 mm with a standard deviation of 4.842 mm. The Rolling Joint model had an average RMSE of 9.962 mm with a standard deviation of 4.395 mm. The Rolling Joint showed the best quantitative agreement with the model, while the Three Position 4-Bar Linkage showed the best qualitative agreement through visual inspection of the ICR movement along the computational curve. These results show a promising future for physical, customizable modeling of an alternative to computational and animal models for VML research.

Keywords: Volumetric Muscle Loss, Gait analysis, Polycentric knee joint, 4-bar linkage, Rolling contact joint, Motion capture

Introduction

Background

Volumetric muscle loss (VML) presents a substantial challenge in both military and civilian medicine, involving the loss of skeletal muscle tissue to an extent that the body cannot regenerate naturally, causing immense functional impairment.[1,2] Understanding VML's effects on gait is critical to the development of treatments and therapies to assist those in recovery. Similarly, understanding the effects of various therapeutic strategies on gait in preclinical testing is critical for developing technologies that can aid humans following a VML injury.

Rat models have been used to study VML due to the kinematic and biomechanical similarities between the rat hindlimb and the human leg.[3] These studies require excision of skeletal muscle and subsequent healing periods before examination and analysis can occur.[4,5] Computational models, such as the one developed by the UVA MAMP Lab in OpenSim, offer precise control of joint dynamics and idealized motion, but fall short in simulating the complexity and variability of the physical world. Real-world factors such as joint compliance and mechanical resistance are difficult to capture in silico. Furthermore, modeling therapeutic strategies or neuromuscular disruptions in a purely digital context does not account for the physical feedback required for testing neural control systems. Therefore, a physical robotic model is necessary to bridge this gap, offering a repeatable, modifiable, and ethically viable platform for experimental design.

Literature Review

VML research has traditionally relied on live animal models to assess muscle regeneration, joint mechanics, and gait recovery.[1,6] These models have historically provided critical insights into the progression and treatment of musculoskeletal disorders due to their biological and biomechanical parallels with human systems. However, ethical concerns, high inter-animal variability, and translational failures have increasingly prompted the scientific community to reconsider their widespread use as the field moves toward the 3Rs (Replacement, Reduction, and Refinement) of animal use, prompting a shift towards research into robotic analogs.[7]

One key driver of robotic model development is the limitation of purely computational simulations. Digital musculoskeletal models, such as those built in OpenSim, allow researchers to simulate limb motion and neural control algorithms in idealized settings. However, these simulations often lack the physical feedback mechanisms necessary to fully predict real-world performance, especially in situations involving mechanical resistance, joint compliance, or sensorimotor delay.[8] For example, in modeling joint articulation or postural control under dynamic loading, the absence of material and force interaction renders digital models insufficient for testing robust therapeutic strategies. Robotic platforms, by contrast, can incorporate real-world physics, offering a more realistic testbed for evaluating control architectures, prosthetic responses, or rehabilitation techniques

These advances are also supported by new technologies in biomechanics and motion capture. Current studies have demonstrated the use of marker-based systems to track skeletal motion in rodents with high precision, providing the quantitative backbone necessary for validating robotic limb trajectories.[8] Combining such tools with robotic limbs can close the loop between design and simulation, ultimately improving our grasp over the physical outcomes of theoretical strategies in research.

Aims

We aim to create a physical, actuatable model that replicates the complex kinematics of a Lewis rat's hip and knee joints, primarily, the polycentric nature of the knee joint and the three degrees of rotational motion of the hip joint. We also aim to develop rudimentary actuation techniques for the model by averaging muscle groups to simplified representations that can be expanded later. By being able to "turn on" and "turn off" muscle actuators, researchers can mimic skeletal muscle injuries without the financial and time costs of live rat studies, and the inaccuracy of simulations. Fine tuning allows for a wide breadth of injury and therapeutic strategy modeling. This physical model will thus accelerate VML research, and aid in developing novel treatments for those suffering VML and other musculoskeletal conditions. It was expected that a 4-Bar Linkage model designed around an average of the instantaneous center of rotations of anterior and posterior points on the tibia would most accurately mimic the polycentric movement of the knee joint.

Design Constraints/Assumptions/Limitations

All designs were inspired by the MAMP Lab's computational model of a Lewis Rat Hindlimb. The model existed in OpenSim 4.5 and included bone anatomy, simulated muscles, and constrained joint articulations. A motion file extending the tibia from 20 to 150 degrees in relation to the femur was provided and used in connection with markers to collect position data to inform the physical model's design.

Design constraints included scaling mechanical components to match rat proportions, implementing physiologically accurate insertions to mimic proper joint behavior, and the integration of actuation systems for simulation of muscle contraction and relaxation. Analysis of the knee kinematic accuracy was assessed in the sagittal plane only, but methods for further study involving mediolateral rotation are discussed in the conclusion.

Design Methodology

4-Bar Linkage Designs

A 4-bar linkage is a commonly used mechanism that can achieve constrained translational and rotational movement. The linkage assembly is made up of 4 rigid links connected by rotating pin joints, forming a closed loop. To approximate the computational model's polycentric motion, two 4-bar designs were created. Anterior and posterior markers were attached to the proximal end of the tibia on the computational model and served as two pin locations for the 4-bar joint. Their x and y coordinate positions were tracked through the joints full range of motion from 20 in the flexed position to 150 degrees in the extended position. For the Three Position 4-Bar Design, the ICR was calculated using the coordinates of the anterior and posterior makers at three angles: 20, 85, and 150 degrees between the tibia and femur. A geometric representation of the method is shown in Figure 1a, where the ICR is at the intersection of perpendicular bisectors of the vectors connecting consecutive positions. The center of rotation point for the anterior and posterior markers was used for the remaining two pin locations on the Three Position 4-Bar Design (Figure 1b). For the Average ICR 4-Bar Design, the instantaneous center of rotation for each anterior and posterior tibia point was measured between consecutive positions at 5-degree increments over the full range of motion from 20 to 150 degrees. The average location of the anterior and posterior ICR points were calculated and used as the positions for the remaining two pin locations for the Average ICR 4-Bar Joint (Figure 1c).

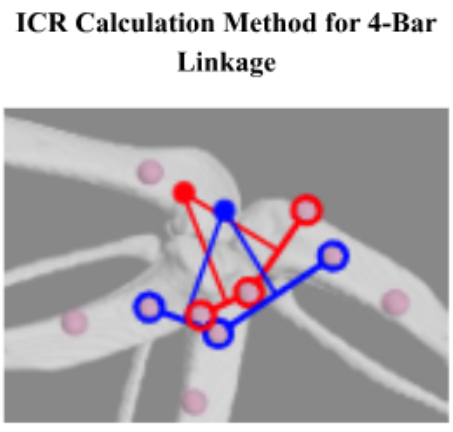

Fig. 1a. Geometric representation of point center of rotation calculation for 4-bar design using anterior and posterior tibia markers. The intersection of perpendicular bisectors of the vectors connecting consecutive positions is the ICR.

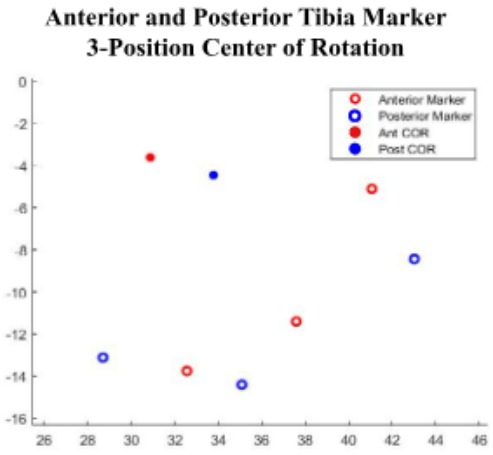

Fig. 1b. Coordinate locations for the anterior and posterior tibia markers at 20, 85, and 150 degrees with corresponding center or rotation points.

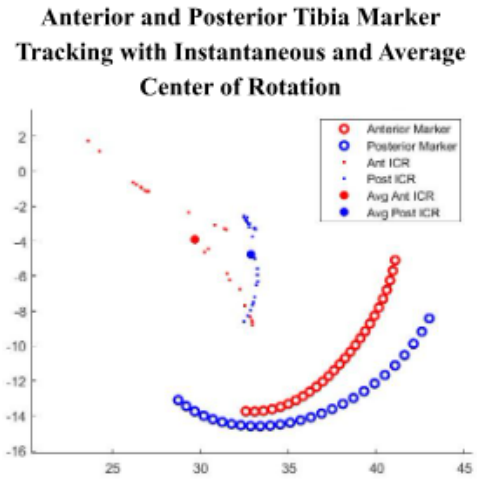

Fig. 1c. Coordinate locations for the anterior and posterior makers from 20 to 150 degrees with ICRs and average COR.

Rolling Contact Knee Joint Design

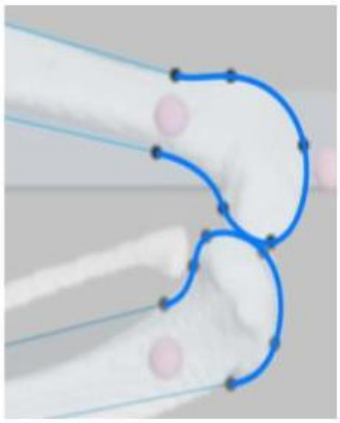

Fig. 2a. Rolling contact joint surface boundary tracing.

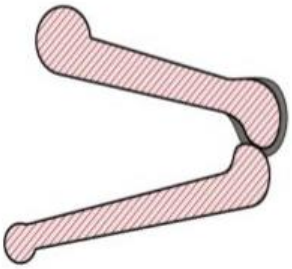

Fig. 2b. Cross section of rolling contact joint design.

Fig. 2c. Front view of ACL/PCL tendon weave.

Fig. 2d. Back view of ACL/PCL tendon weave.

Rolling Contact Joint Design

From a lateral view, the femoral and tibial condyle surface boundaries on the computational model were traced in Fusion360 (Figure 2a). The traced profiles were extruded to form 3-D surfaces that articulate on each other to mimic the physiology of a natural knee joint (Figure 2b). To constrain the joint, grooves were designed into the femur and tibia to allow string to be woven through in a figure eight pattern to approximate the function of the anterior (ACL) and posterior cruciate ligaments (PCL). Front and back views are shown below (Figure 2c, Figure 2d). Cylindrical extrusions for motion capture marker alignment were attached to ensure consistency with computational model positions (Figures 3a).

Knee Actuation

To actuate the knee, muscles controlling the joint were grouped into one representative flexor actuator, and one representative extensor actuator. Each actuator consisted of a servo motor with a round horn attached. The servo horn served as one attachment point for braided nylon cord on the femur, and an eye hook served as the other attachment point on the tibia (Figure 3a). Eye hooks were used to guide the cord actuators between the attachment points. To extend the knee joint, the extensor servo was contracted while the flexor servo was relaxed. To flex the joint, the flexor servo was contracted while the extensor servo was relaxed.

Hip Multi-Axis Rotation Design and Actuation

To achieve rotation motion in three axes, servo motors were connected in series to each other orthogonally (Figure 3b). The three motors represented groupings of hip flexors/extensors, abductors/adductors, and rotators.

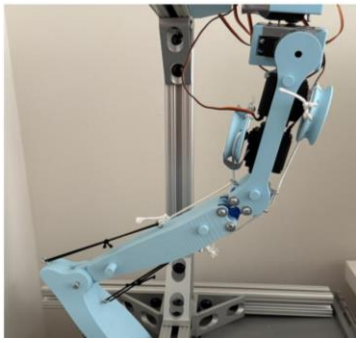

Fig. 3a. Knee Actuator Attachment and Wrapping Points. Attachment points for the knee flexors and extensors are on the servo horns connected to the femur and eye hooks on the tibia; Wrapping points are connected to eye hooks on the femur.

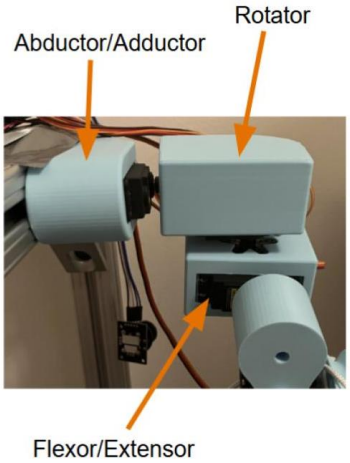

Fig. 3b. Multi-Axis Hip Design. Hip Design with hip muscle groups approximated in 3-axis servo setup.

Knee Kinematic Validation

To validate the polycentric motion of the knee joint, the ICR of the computational model and the physical model were measured. On the computational model, distal and proximal markers were added to the ends of the femur and the tibia (Figure 4). The tibia was rotated from 20 to 150 degrees while the femur remained static, and the ICR of the tibia body was calculated using the distal and proximal marker coordinates tracked at 5-degree increments (Figure 5). A graphical representation of the method is shown in Figure 4 and calculation shown in Appendix A.

The locations of the tibia and femur proximal and distal marker locations were translated to the physical model, and reflective markers were placed on those locations for motion capture (Figure 6). On the physical model, the femur was held in place and the tibia rotated through its range of motion while motion capture cameras captured the positions of the four markers.

The physical model data was normalized to the computational model by aligning the femur anterior and posterior points. As the computational data was captured at 5-degree increments, the physical marker data for each angle between 20 and 150 degrees at 5-degree increments +/- 0.5 degree were averaged together to get points for comparison. Using the average anterior and posterior tibia points for each incremental position, the body ICR was calculated following the same method in Appendix A.

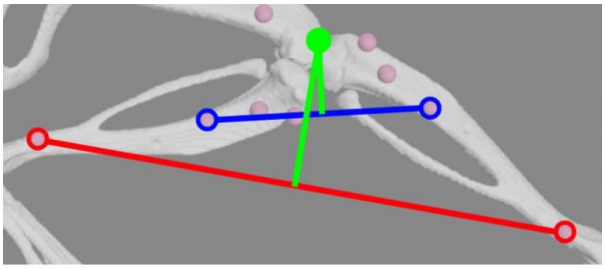

Fig. 4. Proximal and Distal Tibia Point Selection and Knee ICR Calculation Method. Geometric representation of body center of rotation calculation using proximal and distal tibia markers in consecutive positions.

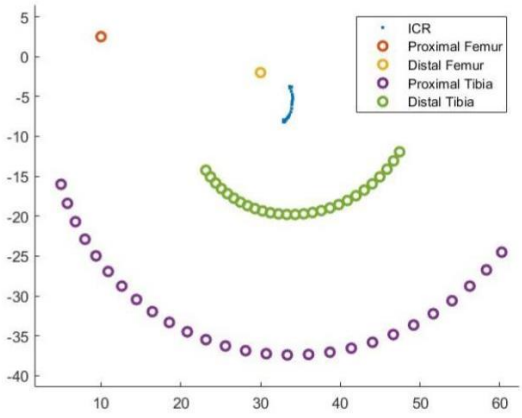

Fig. 5. Computational Model to Marker Data and ICR from 20 to 150 Degrees. The proximal and distal markers on the femur were used to calculate the ICR of the knee joint on the computational model while the femur remained static.

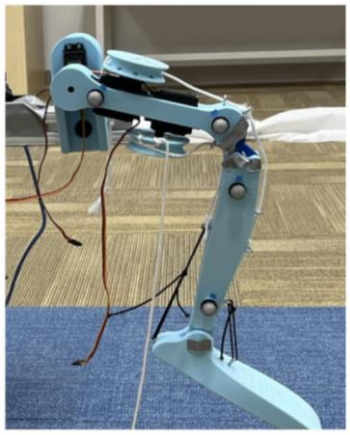

Fig. 6. Physical Hindlimb with Motion Capture Markers Attached. Physical model set up for motion capture data recording with proximal and distal femur and tibia markers.

Results

Three trials were performed for each prototype for a total of nine trials. A comparison of the ICR from the computational model versus the ICR from the Average ICR 4-Bar Linkage Model can be seen in Figure 7a**.** While there is some polycentric movement, the ICR points seem to be located mainly in a grouping to the left of the computational curve with some points traveling up along the curve towards its end. Figure 7b shows that there is a relatively consistent magnitude of the RMSE in the x-axis but it appears to start positive and become negative as the points progress up the curve. The y-axis shows a similar but opposite trend with the beginning points having a negative RMSE but becoming more positive as the position progresses. Overall, the RMSE is kept under 20 mm and the graph shows a general polycentric nature of the model.

The Three Position 4-Bar Linkage model shows a significant improvement of the qualitative analysis of the polycentric curve (Figure 11). Figure 7c shows that there is a strong correlation with the progression of the points mapping up along the computational model curve. While there are some outliers, generally the points follow the curved arc to a close degree giving a strong indication of the polycentric nature of the joint. Figure 7d shows that there is very little error up to around point 15 when there is a dramatic shift in both the x-axis and the y-axis with large errors in the positive and negative directions. This increases the average error of the model up to a high degree. However, qualitatively this model seems to follow the polycentric curve the best.

The rolling contact joint ICR points can be seen in Figure 7e**.** This model shows a large grouping towards the bottom of the computational curve without distinct clear signs of a mobile polycentric nature; however there does appear to be some movement along the ICR curve, especially with the last few points. The RMSE of these points shows promising results with all of them following under 10 mm for both the x-axis and the y-axis as can be seen in Figure 7f.

The nine total trials and their averages can be seen clearly in Figure 8. The rolling joint has the lowest RMSE average error at 9.963 mm followed closely by the Average ICR 4-Bar Linkage Model at 11.344 mm. The Three Position 4-Bar Linkage model had the highest average at 18.294 mm with a noticeably larger standard deviation at 4.842 mm. The Rolling Joint Model also had a noticeably large standard deviation at

44.395 mm with the 4-Bar Linkage 1 with the smallest standard deviation of 1.048 mm.

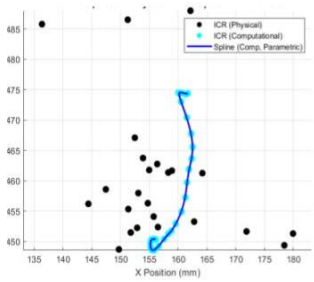

Fig. 7a. ICR Comparison Average 4-Bar Linkage Physical vs Computational Models. ICR Comparison of Average ICR 4-Bar Linkage model to the computational model.

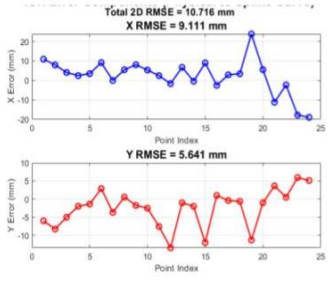

Fig. 7b. ICR 2D Error Components for Average 4-Bar Linkage model. Root mean squared error by point separated along x-axis and y-axis

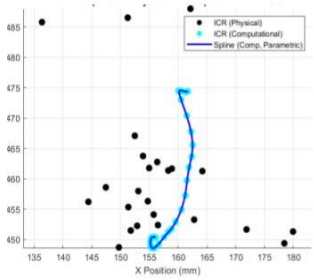

Fig. 7c. ICR Comparison 3 Position 4-Bar Linkage Physical vs Computational Models. ICR Comparison of 3 Position ICR 4-Bar Linkage model to the computational model.

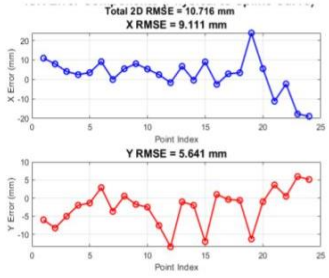

Fig. 7d. ICR 2D Error Components for 3 Position 4-Bar Linkage model. Root mean squared error by point separated along x-axis and y-axis

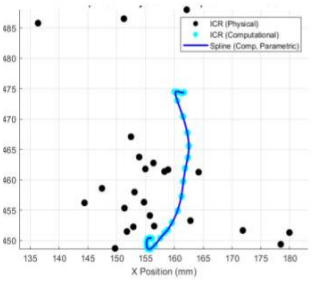

Fig. 7e. ICR Comparison Rolling Contact Joint Physical vs Computational Models. ICR Comparison of Rolling Contact Joint model to the computational model.

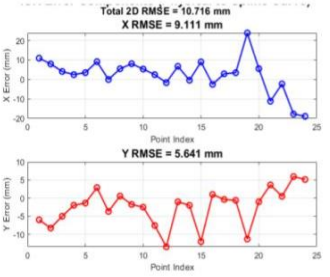

Fig. 7f. ICR 2D Error Components for Rolling Contact Joint model. Root mean squared error by point separated along x-axis and y-axis

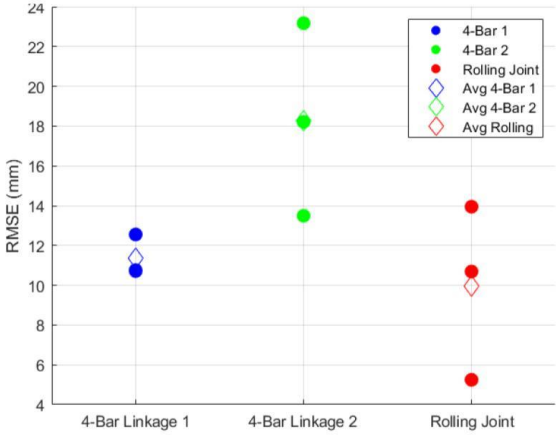

Fig. 8. RMSE Comparison Across Models. The average 2D RMSE of the ICR points from the computational model curve for each trial and the average of the three trials for the three models

Discussion

Primary Takeaways

Consistency

The Average ICR 4-Bar Linkage model showed the most consistency of the three models with a clearly smaller standard deviation. However, with only three trials per model, it would be best for more repeated trials to happen to confirm the significance of its lower standard deviation. If, indeed, this model does have a lower standard deviation, it could be for several reasons not necessarily relating to the location method of calculating the pins. For example, this model could have had better margins for the pins connecting the joint together allowing for more consistent motion. While it's promising to have such consistency in the model, it may not be necessarily due to the type of joint used and more related to the construction of the prototype.

Quantitative Success

The error of the ICR points to the computational model was the main area of concern for the experiment. This had a clear favorite with the lowest area found with the Rolling Joint model. However, while root mean square error is an effective analytical tool to easily illustrate the ability of the joint to match the computational model, it heavily favors the error of outliers and does not account for where the point should be at that particular angle in the gait cycle. Future research should compare the ICR points through a point-to-point method between the computational model and physical model. This would allow for outliers that continue past the gate of the knee to not be continued towards the error as well as better reflecting the movement through time of the gait cycle of the ICR points that is desired in the polycentric joint.

Qualitative Success

Finally, qualitatively it appears that the Three Position 4-Bar Linkage model followed the polycentric curve the best despite its higher RMSE values. The comparison graph shows a clear movement of ICR points along the computational curve and even extending past it. This analysis shows that visually speaking the Three Position 4-Bar Linkage model follows the polycentric nature of the computational model the best.

Overall Success

Both the Three Position 4-Bar Linkage and the Rolling Joint model show a lot of promise for future iterations to be developed. The Rolling Joint has a low error associated with it showing it matched the rotational points

of the computational model well. The Three Position 4-Bar Linkage model shows a visually appealing polycentric nature that could be further refined with point selection to accurately mimic the polycentric nature of a physiologically accurate knee joint.

Future Direction

Future iterations of this project could include several upgrades to enhance the accuracy and functionality of the model in research. Among these improvements, the most promising would be the inclusion of stepper motors or linear actuators to improve joint precision and stability. Stepper motors provide far more positional control than our current servos, and would be able to replicate isometric tensioning in muscle simulation, drastically enhancing the functionality of our model for orthopedic research. Alternatively, pneumatic and electro-hydraulic artificial muscles stand out as early developmental stage options for more robust and biologically inspired contraction kinematics.

For the knee joint, replacing the fixed pin joints in the 4-bar linkage with guided slots or compliant elements could benefit the polycentric tracking's accuracy, especially outside of the sagittal plane. Similarly, the rolling contact joint could be reprofiled to accommodate mediolateral motion to better simulate cartilage contact forces, serving as a more accurate analog to the actual rat knee structure.

In terms of hip actuation, development of a ball-and-socket joint with a cable-driven actuation system could provide for a far more continuous and natural three-dimensional rotation. A ball-and-socket joint would allow for a more anatomically faithful torque transmission, especially if the design incorporated damper mechanisms to simulate the passive joint stiffness of the hip.

A notable improvement to the design would certainly be the addition of finer control over muscle grouping, which would be done by segmenting actuator control to individual muscle analogs rather than compiling flexors and extensors together. This design change would allow for the simulation of partial injury and selective neural inhibition, making it far more applicable to VML cases overall. Also, the integration of feedback systems using IMUs or strain sensors could allow the model to autonomously adjust its actuators based on positional errors or gait phase, allowing the model to more closely mimic in vivo conditions.

Conclusions

The physical modeling of the rat hindlimb successfully captured the key biomechanical features of the polycentric knee joint and the multi-axis hip. Among the knee joints, the Rolling Joint model had the lowest average RMSE of 9.963 mm, suggesting that it has the best quantitative agreement with the computational model. The Three Position 4-Bar Linkage showed the strongest qualitative agreement with a clear visual comparison of the polycentric motion, albeit with the highest RMSE of 18.294 mm. Finally, the Average ICR 4-Bar Linkage model had the smallest standard deviation of 1.048 mm showing the most consistent performance out of the three models. Error analysis shows that future experiments could utilize a more accurate error calculation that follows the polycentric movement along the curve better than RMSE. However, the models show strong foundations for future developments with satisfying mimicking of the polycentric nature of the knee joint. Ultimately, this shows that physical modeling offers a promising alternative to purely computational models for VML research that can allow for customizable injury simulation and potential for preclinical therapy testing without live animal use.

References

1. Downing, K., Prisby, R., Varanasi, V., Zhou, J., Pan, Z., & Brotto, M. (2021). Old and new biomarkers for volumetric muscle loss. Current opinion in pharmacology, 59, 61–69. https://doi.org/10.1016/j.coph.2021.05.001
2. Testa, S., Fornetti, E., Fuoco, C., Sanchez-Riera, C., Rizzo, F., Ciccotti, M., Cannata, S., Sciarra, T., & Gargioli, C. (2021). The War after War: Volumetric Muscle Loss Incidence, Implication, Current Therapies and Emerging Reconstructive Strategies, a Comprehensive Review. Biomedicines, 9(5), 564. https://doi.org/10.3390/biomedicines9050564
3. Grogan, B. F., Hsu, J. R., & Skeletal Trauma Research Consortium (2011). Volumetric muscle loss. The Journal of the American Academy of Orthopaedic Surgeons, 19 Suppl 1, S35–S37. https://doi.org/10.5435/00124635-201102001-00007
4. Christ Lab (2024). VML Injury. https://christlab.org/vml-injury/
5. Grogan, Brian F. MD; Hsu, Joseph R. MD Skeletal Trauma Research Consortium. Volumetric Muscle Loss. American Academy of Orthopaedic Surgeon 19():p S35-S37, February 2011.
6. Dienes, J. A., Hu, X., Janson, K. D., Slater, C., Dooley, E. A., Christ, G. J., & Russell, S. D. (2019). Analysis and Modeling of Rat Gait Biomechanical Deficits in Response to Volumetric Muscle Loss Injury. Frontiers in bioengineering and biotechnology, 7, 146. https://doi.org/10.3389/fbioe.2019.00146
7. Hubrecht, R. C., & Carter, E. (2019). The 3Rs and Humane Experimental Technique: Implementing Change. Animals : an open access journal from MDPI, 9(10), 754. https://doi.org/10.3390/ani9100754
8. Marx, U., Andersson, T. B., Bahinski, A., Beilmann, M., Beken, S., Cassee, F. R., Cirit, M., Daneshian, M., Fitzpatrick, S., Frey, O., Gaertner, C., Giese, C., Griffith, L., Hartung, T., Heringa, M. B., Hoeng, J., de Jong, W. H., Kojima, H., Kuehnl, J., Leist, M., … Roth, A. (2016). Biology-inspired microphysiological system approaches to solve the prediction dilemma of substance testing. ALTEX, 33(3), 272–321. https://doi.org/10.14573/altex.1603161
9. Monsees, A., Voit, KM., Wallace, D.J. et al. Estimation of skeletal kinematics in freely moving rodents. Nat Methods 19, 1500–1509 (2022). https://doi.org/10.1038/s41592-022-01634-9

Appendix

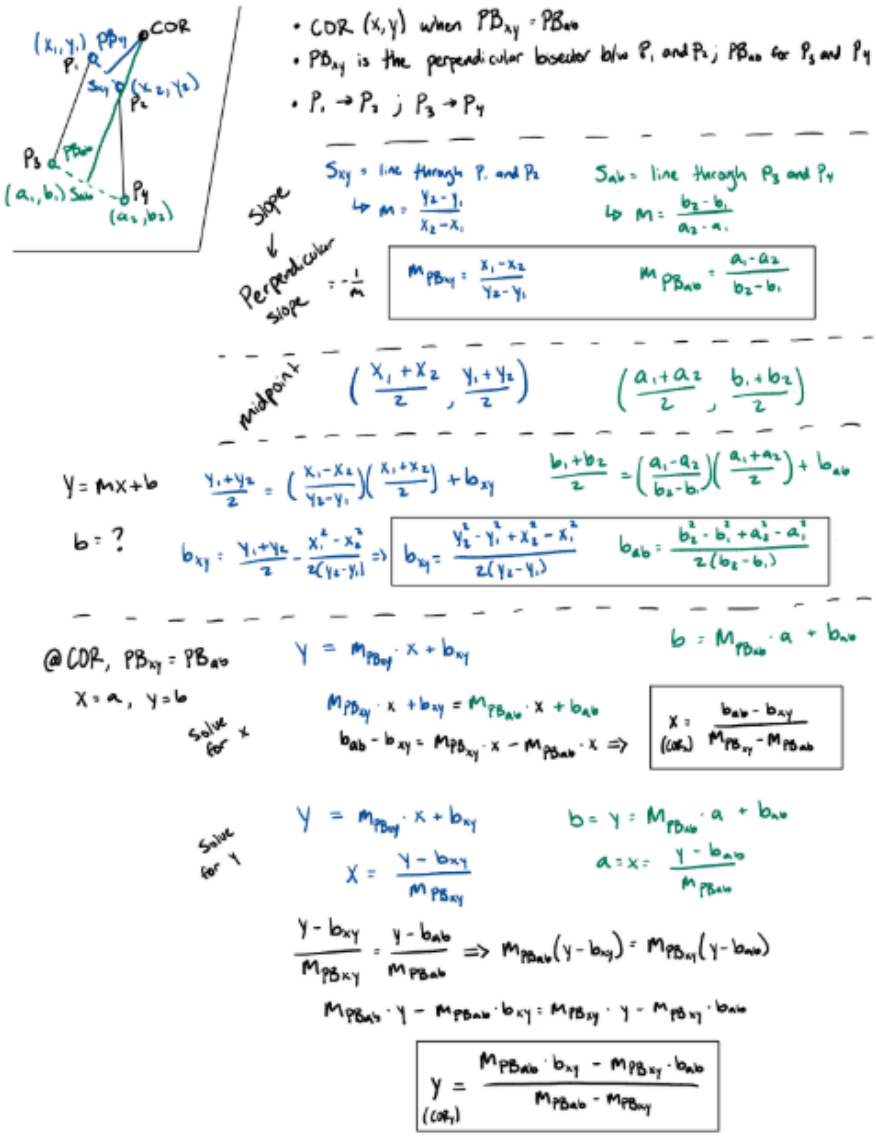

Appendix A. Body Instantaneous Center of Rotation Calculation Method. To calculate the instantaneous center of rotation for a body, two points on a rigid body are tracked between consecutive positions. The intersection of perpendicular bisectors for vectors connecting each point between consecutive positions is the body's center of rotation.